REPORT DOCUMENTATION PAGE

Form Approved
OMB No. 0704-0188

1. REPORT DATE (DD-MM-YYYY)	2. REPORT TYPE	3. DATES COVERED (From - To)
21-06-2004	REPRINT	

4. TITLE AND SUBTITLE
Model and Igniter Development for Plasma Assisted Combustion

5a. CONTRACT NUMBER

5b. GRANT NUMBER

5c. PROGRAM ELEMENT NUMBER
61102F

6. AUTHOR(S)
S. Williams, S. Popovic, L. Vuskovic, C.D. Carter*,
L. Jacobsen*, S. Kuo*, D. Bivolaru*, S.A.P. Corera**,
S.P. Kahandawala**, and S.S. Sidhu**

5d. PROJECT NUMBER
2303

5e. TASK NUMBER
BM

5f. WORK UNIT NUMBER
A4

7. PERFORMING ORGANIZATION NAME(S) AND ADDRESS(ES)

Air Force Research Laboratory
29 Randolph Road
Hanscom AFB MA 01731-3010

8. PERFORMING ORGANIZATION REPORT NUMBER

AFRL-VS-HA-TR-2004-1132

9. SPONSORING / MONITORING AGENCY NAME(S) AND ADDRESS(ES)

10. SPONSOR/MONITOR'S ACRONYM(S)
AFRL/VSBXT

11. SPONSOR/MONITOR'S REPORT NUMBER(S)

12. DISTRIBUTION / AVAILABILITY STATEMENT
Approved for Public Release; Distribution Unlimited

*AFRL/PR, Wright Patterson AFB, OH, **Mechanical & Aerospace Engineering, Univ of Dayton, OH.

13. SUPPLEMENTARY NOTES
REPRINTED FROM: PROCEEDINGS OF 42nd AEROSPACE SCIENCES MEETING AND EXHIBIT, 5-8 January 2004, Reno, NV (AIAA 2004-1012)

14. ABSTRACT

Recent progress on our efforts to develop a detailed kinetic mechanism for C_8H_m hydrocarbons and practical plasma igniters for plasma-assisted combustion are discussed. Shock tube validation experiments made in argon using a fixed stoichiometry ($\Phi = 1.0$), pressures of approximately 0.95 and 1.05 atm, and temperatures ranging from 850 to 1200 K (post reflected shock) are presented. The mechanism is being expanded to include electron kinetics and to allow for a degree of nonequilibrium modeled with separate electron and gas temperatures. Quantum calculations used to derive needed electron impact ionization/dissociation cross-sections for hydrocarbons are discussed. In addition, ignition of ethylene fuel in a Mach 2 supersonic flow with a total temperature of 590 K and pressure of 5.4 atm is demonstrated using a low frequency discharge with peak and average powers reaching 8 kW and 2.8 kW, respectively.

15. SUBJECT TERMS
Ion chemistry Combustion Plasma enhanced combustion Hydrocarbon ions
Plasma torch Shock tube

16. SECURITY CLASSIFICATION OF:			17. LIMITATION OF ABSTRACT	18. NUMBER OF PAGES	19a. NAME OF RESPONSIBLE PERSON
a. REPORT	b. ABSTRACT	c. THIS PAGE			S. Williams
UNCLAS	UNCLAS	UNCLAS	SAR	9	19b. TELEPHONE NUMBER (include area code) 781-377-2076

AFRL-VS-HA-TR-2004-1132

AIAA 2004-1012

Model and Igniter Development for Plasma Assisted Combustion

S. Williams, S. Popovic, L. Vuskovic
Air Force Research Laboratory
Hanscom AFB, MA

C. Carter, L. Jacobson, S. Kuo, D. Bivolaru
Air Force Research Laboratory
Wright-Patterson AFB, OH

S. Corera, M. Kahandawala and S. Sidhu
University of Dayton
Dayton, OH

42nd Aerospace Sciences Meeting & Exhibit
5-8 January 2004
Reno, Nevada

Model and Igniter Development for Plasma Assisted Combustion

Skip Williams,* Svetozar Popovic†, Leposava Vuskovic†
Air Force Research Laboratories, Space Vehicles Directorate
Space Vehicles Directorate, 29 Randolph Road, Hanscom AFB, MA 01731-3010

Campbell D. Carter¶, Lance Jacobson,* Spencer Kuo‡, Daniel Bivolaru‡
Air Force Research Laboratories, Propulsion Directorate
Aerospace Propulsion Directorate, 1950 Fifth St., Wright-Patterson AFB OH 45433-7521

Shehan A. P. Corera[a], Moshan S. P. Kahandawala[a] and Sukh S. Sidhu[a,b]
[a]Mechanical and Aerospace Engineering, [b]Environmental Engineering
University of Dayton, 300 College Park, Dayton, OH 45469-0114

Abstract

Recent progress on our efforts to develop a detailed kinetic mechanism for C_8H_m hydrocarbons and practical plasma igniters for plasma-assisted combustion are discussed. Shock tube validation experiments made in argon using a fixed stoichiometry ($\Phi = 1.0$), pressures of approximately 0.95 and 1.05 atm, and temperatures ranging from 850 to 1200 K (post reflected shock) are presented. The mechanism is being expanded to include electron kinetics and to allow for a degree of nonequilibrium modeled with separate electron and gas temperatures. Quantum calculations used to derive needed electron impact ionization/dissociation cross-sections for hydrocarbons are discussed. In addition, ignition of ethylene fuel in a Mach 2 supersonic flow with a total temperature of 590 K and pressure of 5.4 atm is demonstrated using a low frequency discharge with peak and average powers reaching 8 kW and 2.8 kW, respectively.

Introduction

Airbreathing propulsion at supersonic velocities is subject to the stressing requirement that mixing, ignition, and combustion must take place on very rapid time scales. In terms of combustion performance, the candidate fuel should have overall combustion times in the low-to-sub millisecond range at about 1000 K and 0.5-2 atmospheres. Liquid hydrocarbons have been selected for use by the DoD as the fuels of choice due to their high energy density, excellent storage stability, good cooling capability, and compatibility with the existing fuels infrastructure. Unfortunately, liquid hydrocarbon fuels do not meet the necessary combustion time characteristics, thus placing emphasis on combustion enhancement techniques. A number of such methods have been suggested and explored to varying degrees. Hot gas piloting, photo irradiation, energy intensive ignition sources (e.g., laser, plasma), heterogeneous catalysts, and homogeneous catalysts are typical of the techniques that have been considered for combustion enhancement, particularly under conditions where ignition would not otherwise occur. However, a major hurdle for success of any of the above mentioned combustion enhancement techniques is the lack of combustion data and validated mechanisms at conditions relevant to scramjet operation. This paper describes an experimental and computational program aimed at developing a better understanding of the important and relevant chemistry in these combustion environments.

Neutral Mechanism Validation

Kinetic computations[1] regarding the ignition of a mixture of isooctane and ethylbenzene, a kinetic surrogate for jet fuel, indicate that the ignition delay time is reduced by three orders of magnitude from 900 to 1500 K due mainly to the large ignition activation energies, hence steep temperature dependencies, of the large hydrocarbon components of jet fuel. Although these results are informative, these detailed kinetic models – having hundreds of elementary reaction steps – need validation at conditions relevant for a typical hydrocarbon-fueled supersonic combustor startup scenario if they are to be used to guide combustor designs.

The detailed neutral mechanism for isooctane used at the Air Force Research Laboratory (AFRL Mech) is based on the validated[2] n-heptane mechanism

* Member AIAA.
† Permanent address: Department of Physics, Old Dominion University, Norfolk, VA 23529
‡ Permanent address: Department of Electrical & Computer Engineering, Polytechnic University, Six Metrotech Center, Brooklyn, NY 11201
¶ Associate Fellow AIAA

developed by Maurice and coworkers with the addition of several reactions pertaining to the combustion of branched alkanes to model isooctane combustion. Measurements of the spontaneous ignition of isooctane obtained in a rapid compression machine[3] at a pressure of ca. 10 atm over the 900-950 K temperature range have shown good agreement with the modified C/H/N/O mechanism.[1]

The rapid compression machine results, however, are outside of the pressure range of interest for a typical scramjet startup scenario. A recent shock tube study was performed near atmospheric pressure, but the temperatures (1177 to 2009 K) investigated in that study are above typical scramjet startup temperatures.[4] Therefore additional studies were initiated. The shock-tube experiments are technically challenging due to the need to create stable gas mixtures containing condensable components. These experiments were performed in a high purity, turbo-pumped shock tube at the University of Dayton. Measurements were made in argon using a fixed stoichiometry (Φ = 1.0), pressures of approximately 0.95 and 1.05 atm, and temperatures ranging from 850 to 1200 K (post reflected shock). These data are compared to the recent higher-temperature shock tube results of Oehlschlaeger et al. [4].

Isooctane ignition delays were measured using a shock tube equipped with fast-rise-time pressure transducers and optical detectors. The source data was collected on four channels of a digital oscilloscope. Two oscilloscope channels record the pressure measured by the piezoelectric transducers at the sidewall of the test section and at the end plate. The other two channels of oscilloscope record the PMT and photodiode data.

Figure 1 shows sample oscilloscope traces of all four channels of data. A close examination of the end plate pressure transducer trace in Figure 1 shows that reflection of the shock front at end plate generates the desired pressure and temperature (P_5 and T_5) conditions. The pressure trace then stays flat for about 2 ms and then there is another increase followed by a gentle rise leading up to a sharp peak in the pressure trace. The increase in pressure following shock reflection is probably due to reflection from contact surface (interface between driver and driven gases).[5] The gentle rise after contact surface reflection is due to deflagration which was also observed in a previous shock tube study of isooctane ignition conducted by Fieweger and coworkers.[6] The advent of deflagration coincides with the initial rise in CH-band emission at 431 nm (PMT channel), and there is a small but noticeable rise in pressure associated with the leading edge of the CH emission. The rapid pressure rise resulting in the pressure peak signifies a homogenous ignition (detonation), and its start is consistent with the rise in photodiode signal and peak in the CH emission trace. There is good correlation between the times of the rapid rise of all four traces upon fuel ignition although it is noted that the peak measured by the sidewall transducer is typically delayed with respect to the endplate transducer due to the transit time of the detonation wave. Examination of oscilloscope traces of all experiments showed that start of pressure peak due to ignition was consistent with the rise in the photodiode and CH emission signals. Since the photodiode signal produces the sharpest signature in time, the ignition delay times (τ_{ign}) in this study were taken as the time interval from the moment the shock was reflected at the end plate to the moment the photodiode signal rise was observed (as indicated in Fig. 1).

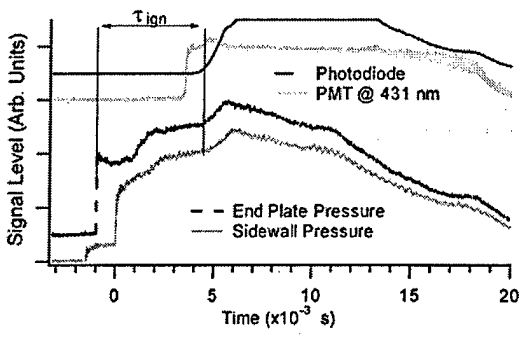

Figure 1: Example oscilloscope traces from isooctane ignition experiment showing pressure transducers, PMT and photodiode data at T_5 = 939 K and P_5 = 1.01 atm.

Before the ignition delay data from this study could be compared to data from other isooctane ignition studies, the increase in P_5 (and thus T_5) due to reflection from the contact surface was quantified. This task was accomplished by repeating selected experimental conditions without any isooctane in the test section. Oxygen was used to make up the small fraction of isooctane (1.48%) and the tested mixtures were 80% Ar and 20% O_2. Assuming isentropic compression, this increase in P_5 was used to calculate T'_5 (γ = 1.38). This increase in P_5 and T_5 is only relevant at T_5 lower than 1075K (τ_{ign} > 2.4 ms), because at higher temperatures ignition is faster and occurs before the reflection from contact surface. In addition, at the higher temperatures the amount of argon in driver gas was also smaller (25% vs. 40%), thus producing a smaller acoustic impedance mismatch between driver and driven gases, (and hence, a smaller reflection from the contact surface).

This increase in P5 and T5 at lower temperatures causes a significant change in conditions of the still unburned gas and leads to shortening of ignition delays. The actual ignition delays for T_5 will be longer and for

T'_5 will be shorter, than those observed in this study. Thus one way treat the data is to plot the observed ignition delay data against both T_5 and T'_5 which will thus provide an upper and lower limit for the actual ignition delays as is done in Figure 1. Note that the data with initial temperature greater than 1075 K $T_5 = T'_5$ and the open and closed symbols are overlapped on the plot.

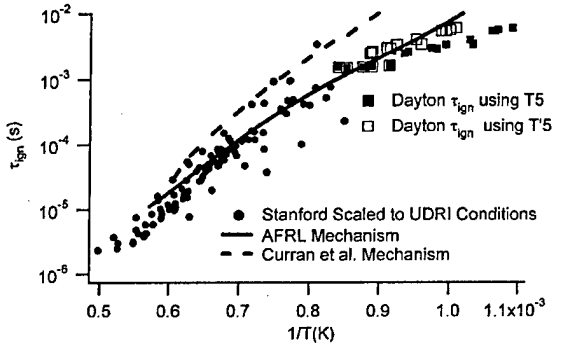

Figure 2: Comparison of isooctane ignition delay times (τ_{ign}) from this study (Dayton) with that obtained in Oehlschlaeger et al. study (Stanford). Solid squares are Dayton ignition delays vs. post-shock temperature (T_5); open squares are ignition delays vs. corrected post-shock temperature (T'_5) and solid circles are Stanford ignition delays. Dashed line depicts AFRL model and solid line depicts results of Curran et al. model.

The shock tube isooctane ignition delay data thus obtained was modeled using CHEMKIN software. Two isooctane kinetic mechanisms, Curran et al.[7] and AFRL Mech, were used to model the experimental data (see Figure 2). Other isooctane kinetic mechanisms (e.g., Davis and Law,[8] Pitsch et al.[9] and Ranzi et al.[10]) are available in literature and were used by Oehlschlaeger et al. to fit their isooctane ignition data. These authors found that all these isooctane models, including one by Curran et al., were able to predict their ignition delay within factor of two but were not unable to capture the temperature dependence exhibited by their experimental data. In this study, just the Curran et al. model is used for comparison as it was readily available and had given comparable fits to the Oehlschlaeger et al. experimental ignition data. The mechanism of Curran et al. was used in conjunction with version 3.7 shock solution of the CHEMKIN software series.[11] AFRL Mech was used in conjunctions with a modified version of the CONP program of the CHEMKIN II software series.[11]

Figure 2 compares the isooctane ignition data from this study (Dayton) with that obtained in Oehlschlaeger et al. study (Stanford). The ignition delay time data from Oehlschlaeger et al. were obtained in 95 total experiments spanning a variety of pressures, equivalence ratios, and oxygen mole fractions in addition to the temperature. These ignition times have been correlated using a regression analysis by these authors and the resulting expression (Eq. 3 of their paper) was used to normalize all of their data to our conditions of 1 atm, equivalence ratio of 1, and 18.52% O_2. Both the Dayton and Stanford data sets are plotted in Figure 2 and exhibit good agreement in the region of 1200 K where the two data sets meet. Also shown in Figure 2 are modeling results obtained using AFRL and Curran et al. mechanisms. The AFRL mechanism shows an excellent agreement with the combined data set (Dayton and Stanford). The Curran et al. mechanism is unable to match the temperature dependence exhibited by both sets of experimental data. Comparison of Dayton and Stanford data also shows that activation energy of ignition at lower temperature (Dayton data) is significantly smaller ~15 Kcal/mol vs. ~ 40 Kcal/mol than that obtained at higher temperatures (Stanford). One explanation of this disagreement is that cool flame and local ignition processes, leading to deflagration rather than detonation, play a significant role in lower temperature ignition and may be responsible for lowering of activation energy. The activation energy of combined data set was calculated to be ~33.6 Kcal/mol which was in good agreement with activation energy of ~ 30 Kcal/mol obtained from AFRL Mech.

Ion Mechanism Validation

In the last Weakly Ionized Gases Workshop, computations regarding the combustion of pure isooctane (i-C_8H_{18}) with a NO^+/e^- ionization scheme[12] and the potential to use resonant enhanced multi-photon ionization (REMPI) to create a large initial concentration of NO^+ and low energy electrons within a shock tube[13] were discussed. The experimental setup has been completed and initial experiments have been performed. In brief, the goal of the experiment is to create a nearly instantaneous initial ionization condition to study the effect of ions and low energy electrons on the ignition delay time of large hydrocarbon fuels. The experimental conditions of the shock-tube measurements are an initial temperature of approximately 1000 K and a pressure of 1 atm. The gas composition in the measurements is 80% Ar, 17.6% O_2, 1.4% isooctane, and 1% NO and the ionization is expected to produce ca. 1-5 x 10^{-4} mole fraction NO^+/e^- during the ca. 5 ns laser pulse duration. Recall that the effects of ionization are most pronounced at lower temperatures. However, the lower limit of the temperature range is determined by the dwell time of the shock tube. A tempera-

ture of 1000 K is low enough to permit the effects of ionization to be observed within the reproducibility of the measurements and high enough to observe the ignition of the isooctane fuel with the present shock tube operating conditions.

The reaction sequences describing the hydrocarbon ionization kinetics added to the detailed hydrocarbon AFRL Mech have discussed previously.[12] In addition, the NOx combustion mechanism of Lindstedt and coworkers[14] and a simple flame ionization mechanism of Pedersen and Brown[15] have also been added. Calculated thermochemical values were used when reliable experimental data was unavailable.[12] Both the detailed reaction mechanism and thermochemical data are available upon request.

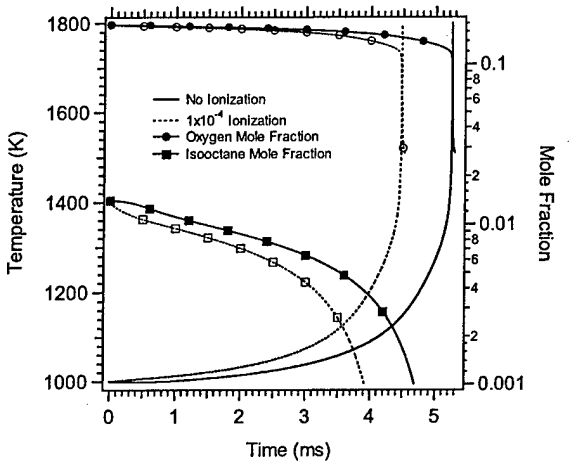

Figure 3. Species concentration and temperature as a function of time for 1.4% i-C_8H_{18}, 17.6% O_2, 1% NO, 80% Ar combustion (Φ=1) at a constant pressure of 1 atm, $T_{initial}$=1000 K with (dashed lines) and without (solid lines) ionization.

Computations are performed for pure isooctane/dry air combustion with a NO^+/e^- ionization kinetics scheme. Results of the computations at 1000 K for isooctane ignition with and without an initial mole fraction ($1x10^{-4}$) of NO^+/e^- are shown in Figure 3. Additional initial conditions include equivalence ratio of Φ = 1.0 and initial pressure of P = 1 atm. The ignition delay time, τ_{ign}, is defined as the time at which the gas reaches a temperature 500 K above the initial value, $T_{initial}$, and is easily seen in the figure as a nearly instantaneous increase in temperature on the millisecond time scale. A 15% reduction in the flame induction time is seen in Figure 3 for an ionization fraction of 10^{-4} relative to the case of no ionization for this example. Larger reductions occur at lower temperatures, higher mole fractions, and leaner fuel mixtures.[1]

Of course, a fundamental difficulty in testing this sort of model is in generating the proper initial condition (e.g., starting out with only NO^+ and "thermal" electrons in the laboratory). Our validation approach involves selectively creating the ion of interest photolytically with a resonant process within a shock tube. For example, NO^+ can be produced using the technique of REMPI.[16] Here, one uses an initial photon to couple to an excited rovibronic state—for example, to the A(v'=0) state with a photon at 226 nm—and a second photon—say at 266 nm, the Nd:YAG fourth harmonic—to photoionize the excited-state molecule; this commonly referred to as a 1+1 REMPI process and is shown schematically in Figure 4. With photons at 226 (for A-X excitation) and 266 nm, the liberated electron will carry away ~0.9 eV of kinetic energy, too little to cause further ionization, but enough to result in some additional rovibrational excitation of collider species. In order to use this approach, it is necessary to "dope" the reactants with a substantial initial concentration of NO, 1%, for example which explains the need to account for the presence of NO in the computation.

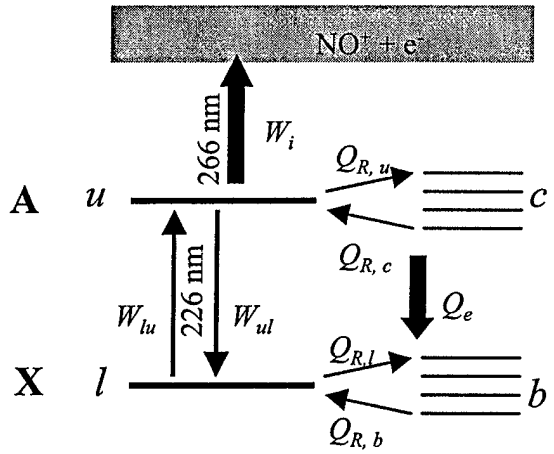

Figure. 4. Energy-level diagram of laser excitation, collisional processes, and photoionization.

Other researches have also used *resonant* photolytic techniques to induce ignition.[17] Often, this has involved the use of a so-called photo-sensitizer gas (e.g., NO_2 or NH_3) which absorbs radiation and dissociates giving a pool of atomic and radical species [e.g., see reference 18]. In other cases, however, one can promote dissociation of the fuel or oxidizer directly, and no sensitizer is needed [e.g., see reference 19]. In one notable study, Forch and Miziolek[20] used a tightly focused 1-mJ 226-nm laser beam (with estimated ir-

radiance of 10^{11} W/cm^2) to induce formation of O atoms and ignition of a room temperature H_2-O_2 mixture. Furthermore, they speculated that O^+ ions and their liberated electrons played a role in the ignition process. In a similar study, Forch and Miziolek[21] found that they could induce ignition with a 243 nm laser beam by tuning it to a two-photon H-atom transition; again, they speculated that a micro-plasma helped promote ignition.

Of course, it is critical to be able to produce NO^+ (or some other ion of interest) efficiently, not only due to the limitations of the available laser system but also due to practical concerns such as shock-tube window damage and fuel photolysis. In the case of NO, this is aided by a reasonably large ionization cross section,[22] $\sigma_{ion} = 7\times10^{-19}$ cm^2 and the large Einstein-B coefficients for the NO $A^2\Sigma^+$–$X^2\Pi$ (0,0) transitions. Furthermore, efficient rotational energy transfer, RET,[23] results in the population adjacent rotational levels, in the case of the A state, and re-population of the directly pumped level, in the case of the X state, both of which are necessary to achieving significant photoionization when coupled with transition saturation.

In the shock-tube experiment, the output of a injection-seeded frequency-doubled Nd:YAG laser (Spectra Physics GCR-170) is passed through a BBO crystal to produce radiation at 266 nm; the two beams are separated with a dichroic reflector and the residual 532-nm beam is used to pump an LAS dye laser The output of the dye laser is frequency doubled with a second BBO crystal and then frequency mixed with the residual fundamental beam from the Nd:YAG laser—using Inrad Autotraker—to produce the 226-nm laser energy to couple the A-X (0,0) band of NO. A delay line is used with the 266-nm beam so that its arrival in the probe region can be varied.

At the time of this publication, the optical setup and experimental timing are complete. Two approximately 5 mm x 1 mm laser sheets at 226 nm and 266 nm with energies of 3 mJ and 60 mJ, respectively arrive 150 μs after the incident shock has reached the end plate. This configuration produces ~ 1×10^{-4} NO^+/e^- ionization mole fraction, and preliminary results indicate that the ignition delay time at 960-975 K is reduced by ~ 300-500 μs in the presence of the laser sheets. More experiments are necessary to acquire sufficient statistics and control experiments are yet to be completed. However, the initial phases of the experiment are going as planned and given the quality of the validation of the neutral mechanism, the results should prove valuable for validating the present mechanism.

Electron Impact Ionization of Hydrocarbons

Our experiments are aimed at producing a single effect at a time in order to isolate the effects of various species, including electrons. However, other researchers are using pulsed nanosecond discharges in shock tubes and are observing interesting results.[24] In these experiments, numerous energetic species are produced, and nonequilibrium between the electrons and heavy particles can be expected. The electrons in these discharges are capable of ionizing, dissociating, or dissociativelly ionizing the molecular species present. While these processes are relatively well understood for air species, they are poorly understood for all but the simplest hydrocarbons.

Rates for the generation of ions by electron impact on hydrocarbon molecules are an important subset of data for chemical kinetic modeling of a wide range the plasma–assisted processes involving hydrocarbons. These data are presently largely unavailable and usually derived indirectly rather than by experiment or calculation. One of the problems in experimental information of fragmentary ionization processes is that practical application usually requires behavior of cross section data at low energies, near the threshold, where current experimental methods are highly inaccurate. On the other hand, the recently calculated values derive from quantum chemistry calculations and yield values of the total ionization cross section in good agreement with experiment;[25] however, procedures able to describe individual fragmentary ion generation are still under development.

Kim and coworkers from NIST have provided a widely applied formula for electron-impact ionization, which they refer as the Binary-Encounter-Bethe model:[25]

$$\sigma_{BEB} = \frac{S}{t+(u+1)/n}\left[\frac{Q\ln t}{2}\left(1-\frac{1}{t^2}\right) + (2-Q)\left(1-\frac{1}{t}-\frac{\ln t}{t+1}\right)\right]$$

where $t = T/B$, $u = U/B$, $S = 4\pi\, a_0^2\, N\,(R/B)^2$, $a_0 = 0.529$ 18 Å, and $R = 13.6057$ eV, B the binding energy, U is the orbital kinetic energy, N the electron occupation number, Q is the dipole constant, and n = 1 for neutral molecules, and n =2 for the singly-charged molecular ion. Dipole constant Q is defined in terms of the continuum dipole oscillator strength df/dW, where W is the kinetic energy of the ionized electron:

$$Q = \frac{2}{N}\int \frac{B}{B+W}\frac{df}{dw}dw$$

By assuming that the asymptotic behavior of oscillator strength in hydrogen, $df/dW \sim (B\text{-}W)^{-2}$ is valid also for at least highly symmetrical hydrocarbon molecules, such as ethylene, one can obtain Q = 1 which simplifies substantially the calculation of the cross section. The total electron-impact ionization cross section is then obtained by summation over all occupied molecular orbitals. Necessary values of B, U, and N are obtained from quantum chemistry calculations and are listed for ethylene in the Table 1.

Table 1. Molecular orbitals, electron binding energy B in eV, orbital kinetic energy U in eV, and electron occupation number N of ethylene.

MO	B	U
1ag	305.51	435.23
1b1u	305.46	435.84
2ag	28.12	41.33
2b1u	21.49	33.78
1b2u	17.44	25.29
3ag	15.97	34.67
1b3g	13.66	28.55
1b3u	10.19	26.59

Total ionization cross section (vs. electron energy) for ethylene is given in Figure 4. The calculated cross sections and the early experimental data by Rapp and Englander-Golden (RGexp)[26] agree well in the threshold region but disagree near the peak. More recently, Tian and Vidal (TVexp)[27] have published tabulated values of dissociative ionization cross sections for electron impact on ethylene in the energy range between 17.5 and 600 eV. Their values for absolute total cross section at high energies are in a good agreement with the calculations. However, values near the threshold are substantially lower. They used the normalization procedure based on the Argon ion counts. Ionization potential of Argon is 15.756 eV, and the low-energy ethylene ions were impossible to account for in that experiment. However, taken together both data sets give very good foundation for the analysis of ethylene ion fragmentation.

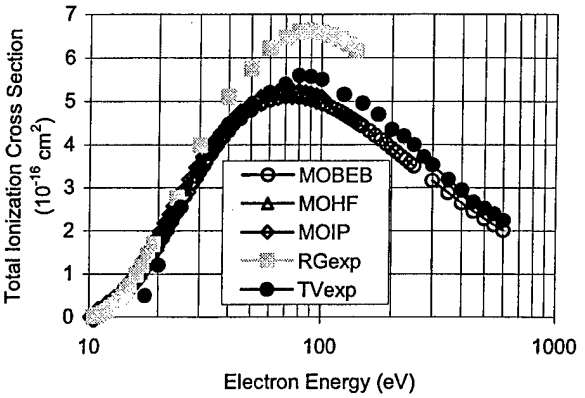

Figure 4. Total ionization cross section for ethylene. MOBEB are the NIST data[25]; MOHF are obtained using the calculated binding energy (10.187 eV) for the HOMO in a Hartree-Fock approximation. MOIP are the data obtained when the calculated binding energy is substituted by the ionization potential (10.51 eV). Experimental values[26,27] are shown as solid symbols.

The procedure has also been applied to n-octane and the result for the total ionization cross section is given in Figure 5. Calculated data reproduce very well the broad maximum of experimental cross section measured by Jiao, DeJoseph, and Garscadden.[28]

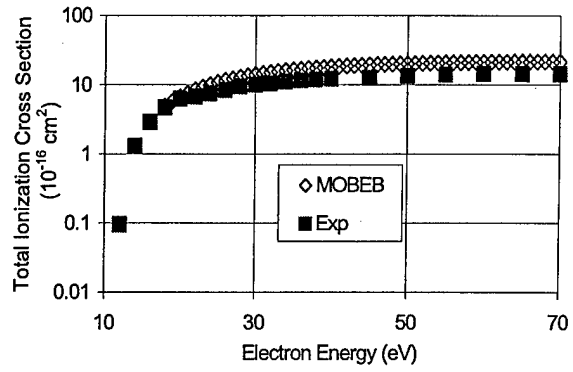

Figure 5. Total cross section for electron impact ionization of n-Octane. Diagram includes present data calculated using molecular orbital parameters (MOBEB) and experimental data by Jiao, DeJoseph, and Garscadden, reference 28.

Plasma Based Igniter

Detailed kinetic modeling using AFRL Mech and the shock-tube validation data described above show that the ignition delay time for isooctane is reduced by three orders of magnitude from 900-1500 K. Additional computations show that a significant decrease in ignition delay time also results when radicals and ionized species are present at mole fractions greater than 10^{-6}. The ignition delay time is decreased most significantly by these species at temperatures lower than 1500 K, suggesting that such processes are particularly important for the initiation of cold fuel-air mixtures. Therefore, ignition aides capable of delivering thermal energy and/or activated chemical species are desired. A DC or low-frequency arc discharge can produce a dense plasma containing significant thermal energy as well as air dissociation products, plasma species, and UV radiation, all of which are beneficial in reducing the ignition delay time. Because of these and other characteristics, such as durability and flexibility, a low frequency, plasma torch module is being explored as a potential ignition aide for supersonics combustors.

In brief, the plasma torch module consists of a cylindrical tungsten central electrode set in a ceramic insulator, which holds the central electrode in place concentrically with respect to the outer ring electrode (stainless steel). The configuration results an annular gap between the ceramic and outer electrode for gas flow. This torch module has a relatively large gap, 2.7 mm, between the electrodes compared to the gap used in non-transferred DC plasma torches, which are usually less than 1 mm. Furthermore, the discharge is restricted to occur outside the module since the ceramic insulator is inserted between the electrodes and all surfaces are flush with respect to each other.

The power supply utilizes a power transformer with a turn ratio of 1:25 to step up the input voltage of 150 V (rms) to 3.75 kV (rms). The input voltage is provided by the single phase 208 V (rms) power line, which is reduced to 150 V (rms) by a Variac. Twelve 1 μF, 2.3 kVAC capacitors are connected to obtain an equivalent 3 μF, 4.6 kVAC rating. This capacitor assembly is connected in series with the transformer and the electrodes. A serially connected diode-resistor assembly is placed in parallel to the electrodes to further step up the peak voltage applied to the electrodes during the reverse bias cycle of the diodes. A resistance of 4 kΩ optimizes the power factor of the power line. Since the resulting RC time constant of 12 ms is longer than the half period of the 60 Hz line input (8.5 ms), the discharge in the torch module occurs in both half cycles (120 Hz operation) regardless of whether the diodes are forward or reverse biased.

The arc loop can be many times the distance between the anode and cathode. The arc loop structure is illustrated in the image (typical of those recorded) shown in Figure 6, which was recorded through a 239 nm interference filter, 10 nm FWHM, with an intensified CCD camera (Roper Scientific PIMAX) set for an 80 ns exposure time. The current loop is coincident with the thin, intense emission loop shown in the figure. For this measurement, pure nitrogen with a pressure of 1.7 atm was supplied to the torch module. The horizontal extent of the arc loop is ca. 3.2 mm, whereas the vertical extent is about 2.5 cm. Such an extended arc loop increases the path length of the charged particles in the discharge by more than 15 times the direct path length from the cathode to the anode. Also shown in Figure 6 is laser-induced fluorescence (LIF) from nitric oxide, NO, obtained using a Nd:YAG-pumped dye laser system to generate laser radiation at 226 nm probing the overlapped $Q_1(12.5)$ and $Q_2(19.5)$ transitions in the $\delta(0,0)$ band of NO. The LIF image appears as the diffuse, less intense background and is best seen on the left side of the figure towards the outer portion of the arc loop. NO is produced within the torch plume in the region where the hot torch gas (pure N_2 was used as the feedstock for this experiment), mixes with quiescent laboratory air. Thus, NO is formed primarily near the outer portion of the arc loop.

The extended arc loop structure produced with this torch module has several distinct advantages. For instance, such images indicate that high-temperature, dissociated, and ionized air extends well above the surface of the torch module, which is important for ignition applications. Furthermore, the conversion of electrical energy to plasma energy may be enhanced due to the longer interaction region.

The time varying voltage V and current I of the discharge were measured using a digital oscilloscope for each supply pressure p_0 in the range from 1.2 atm to 7.6 atm. The product of the V and I functions gives the instantaneous power function. Integrating the power function over one cycle determines the cycle energy of the torch, i.e., the energy carried by torch plasma in each cycle. The results show that this cycle energy varies with the pressure p_0. In the regime of subsonic flow, the cycle energy increases to the maximum of about 28 J at $p_0 = 2.4$ atm. The cycle energy increases again in the supersonic flow regime and reaches a maximum of about 46 J at $p_0 = 6.4$ atm.

Initial evaluation of plasma-assisted ignition was conducted in a supersonic, Mach 2 flow facility with heated air at a total temperature and pressure of 590 K and 5.4 atm, respectively. The resulting static temperature was thus ~330 K, still a relatively low value insofar as ignition is concerned. This facility allows testing of

an individual concept with both gaseous and liquid hydrocarbon fuels without a cavity flame-holder. In the tested configuration, a 15.2 x 30.5 cm test section floor plate fits into a simulated scramjet combustor duct with an initial duct height of 5.1 cm. At the upstream edge of the test section insert, the simulated combustor section diverges on the injector side by 2.5 degrees. This particular hardware was intentionally designed not to study main-duct combustion (ignition of the entire duct), but to reduce the chance of causing main-duct combustion by limiting the equivalence ratio of the tunnel below 0.1. In particular, this was accomplished by placing the fuel injector at the centerline of the tunnel and not employing any flame-holding mechanisms such as a cavity or backwards-facing step. This approach allows the interactions of the fuel plume with the plasma torch to be studied by itself, and any flame produced is strictly created by this interaction, hence decoupling the ignition and flame holding problems as much as possible from the combustor geometry. Tests have been conducted using gaseous ethylene fuel, with a 15 deg downstream-angled single hole.

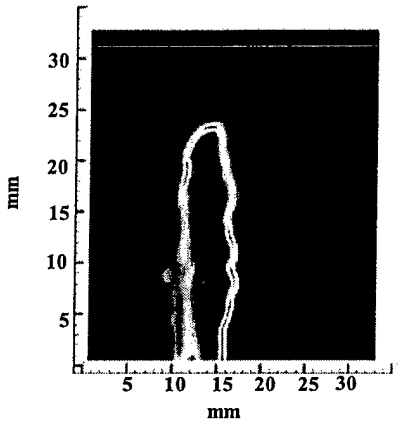

Figure 6. False-color image of an arc loop in torch plasma taken by an intensified CCD camera with an 80 ns exposure though a 239 nm interference filter, 10 nm FWHM. The diffuse emission surrounding the arc loop is from NO laser-induced fluorescence (see text).

The 120 Hz plasma torch module was evaluated and was found to produce a substantial flame plume as observed both from flame chemiluminescence and OH planar laser induced fluorescence (discussed in a future publication). The flame chemiluminescence (blue emission in the tail of the plume) is illustrated in Figure 7, which shows a single frame taken from video recordings of the 120 Hz plasma torch in operation 5 cm downstream of the ethylene-fueled single-hole injector. Several feedstock flow rates were tried over the torch module operational range and a flow rate of ~500 SLPM was determined to produce the largest visible flame for the current electrode configuration. Air produced a larger flame when compared to nitrogen as the torch feedstock. This difference in flame size indicates that this type of flame is very sensitive to the local equivalence ratio and coupling of the ignition source with the mixture.

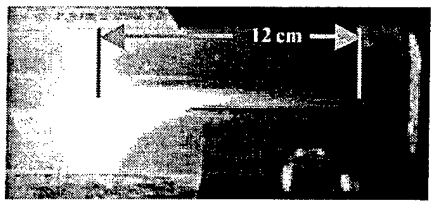

Figure 7. Single frame of flame chemiluminescence viewed from the top taken from video recordings of the 120 Hz plasma torch in operation 5 cm downstream of the ethylene-fueled single-hole injector. Fuel (5.3 gm/sec, 318 K), Freestream (5.4 atm, 586K), Torch (5 kW Peak, 470 SLPM Air).

Conclusions

Models for plasma-based ignition, piloting, and combustion enhancement are useful toward guiding scramjet combustor design and development efforts. Techniques for improving hydrocarbon fuel ignition characteristics have been shown to be enabling for viable hypersonic vehicles powered by scramjets. The efforts described in this contribution will be useful toward the design of efficient combustors for hypersonic propulsion systems. Moreover, the model development effort will facilitate our understanding of the detailed chemistry involved in these evolving technologies. Finally, since the methods being pursued are based on detailed fundamental kinetics treatments, the models developed within this program are broadly applicable to a range of diverse problems such as combustors for gas turbine engines, diesel engines, environmentally clean combustion, spark inhibition, and explosion limits in blended fuels.

Acknowledgements

The authors thank R. P. Lindstedt, L. Q. Maurice, and T. Edwards for helpful discussions and for providing the submechanisms used in this work. The technical support of J. Williamson is gratefully acknowledged. The financial support of the Air Force Office of Scientific Research (AFOSR) and the Nunn Program Office are gratefully acknowledged.

References

[1] S. Williams, A. J. Midey, S. T. Arnold, P. M. Bench, A. A. Viggiano, R. A. Morris, L. Q. Maurice, and C. D. Carter, 9th International Space Planes and Hypersonic Systems and Technologies Conference **AIAA 99-4907** (1999).

[2] D. F. Davidson, D. C. Horning, and R. K. Hanson, **AIAA 99-2216** (1999).

[3] J. F. Griffiths, P. A. Halford-Maw, and C. Mohamed, Combust. Flame **111**, 327 (1997).

[4] M. A. Oehlschlaeger, D. F. Davidson, J. T. Herbon, and R. K. Hanson, Int. J. Chem. Kinet. **36**, 67 (2003).

[5] D. H. Napier and J. R. Simonson, ARS Journal, 1736 (1963).

[6] K. Fieweger, R. Blumenthal, and G. Adomeit, Combust. Flame **109**, 599 (1997).

[7] H. J. Curran, P. Gaffuri, W. J. Pitz, and C. K. Westbrook, Combust. Flame **129**, 253 (2002).

[8] S. G. Davis and C. K. Law, Proc. Comb. Inst. **27**, 521 (1998).

[9] H. Pitsch, N. Peters, and K. Seshadri, Proc. Comb. Inst. **26**, 763 (1996).

[10] E. Ranzi, T. Faravelli, P. Gaffuri, A. Sogaro, A. D'Anna, and A. Ciajolo, Combust. Flame **108**, 24 (1997).

[11] R. J. Kee, F. M. Rupley, and J. A. Miller, CHEMKIN II: A Fortran Chemical Kinetics Package for the Analysis of Gas Phase Chemical Kinetics (Sandia National Laboratories, Livermore, CA, April 1992).

[12] S. Williams, T. M. Miller, W. B. Knighton, A. J. Midey, S. T. Arnold, A. A. Viggiano, and C. Carter, 41st Aerospace Sciences Meeting & Exhibit **AIAA-2003-0704** (2003).

[13] C. Carter, S. Williams, L. C. Lee, S. Sidhu, and J. Graham, 41st Aerospace Sciences Meeting & Exhibit **AIAA-2003-0703** (2003).

[14] R. P. Lindstedt and L. Q. Maurice, Combust. Sci. and Technol. **107**, 317 (1995); R. P. Lindstedt and L. Q. Maurice, Combust. Sci. and Technol. **120**, 119 (1996); L. Q. Maurice, Ph.D. Thesis, Unversity of London, 1996.

[15] T. Pedersen and R. C. Brown, Comb. and Flame **94**, 433 (1993).

[16] V. S. Letokhov, V. I. Mishin, and A. A. Puretzky, Progress in Quan-tum Electronics **5**, 139 (1977).

[17] R. G. W. Norrish, Proc. Comb. Inst. **10**, 1 (1965).

[18] M. Lavid and J. G. Stevens, Combust. and Flame **60**, 195 (1985).

[19] M.-S. Chou and T. J. Zukowski, Comb. and Flame **87**, 191 (1991).

[20] B. E. Forch and A. W. Miziolek, Combust. Sci. and Tech. **52**, 151 (1987).

[21] B. E. Forch and A. W. Miziolek, Combust. and Flame **85**, 254 (1991).

[22] H. Zacharias, R. Schmiedl, and K. H. Welge, Appl. Phys. Lett., 127 (1980).

[23] T. Ebata, Y. Anezaki, M. Fuji, N. Mikami, and M. Ito, " Chem. Phys. 84, Chem. Phys. **84**, 151 (1984); A. Sudbo, S. and M. T. Loy, J. Chem. Phys **76** (3646-3654) (1982).

[24] S. A. Bozhenkov, S. M. Starikovskaia, and A. Y. Starikovskii, Combust. and Flame **133**, 133 (2003).

[25] W. Hwang, Y.-K. Kim, and M. E. Rudd, J. Chem. Phys **104**, 2956 (1996); Y.-K. Kim, W. Hwang, N. M. Weinberger, M. A. Ali, and M. E. Rudd, J. Chem. Phys **106**, 1026 (1997).

[26] D. Rapp and P. Englander-Golden, J. Chem. Phys **43**, 1464 (1965).

[27] C. Tian and C. R. Vidal, Chem. Phys. Lett. **288**, 499 (1998).

[28] C. Q. Jiao, C. A. DeJoseph, Jr., and A. Garscadden, AIAA 4th Weakly Ionized Gases Workshop **AIAA 2001-2950** (2001).